Resident and recruited macrophages differentially contribute to cardiac healing after myocardial ischemia

Tobias Weinberger[1,2,3,4], Denise Messerer[1,2], Markus Joppich[5], Max Fischer[1,2,3], Clarisabel Garcia[4], Konda Kumaraswami [1,2], Vanessa Wimmler[1,2], Sonja Ablinger[1,2], Saskia Räuber[1,2,6], Jiahui Fang[1,2], Lulu Liu[1,2], Wing Han Liu[1], Julia Winterhalter[1,2], Johannes Lichti[1], Lukas Tomas[1,2,3], Dena Esfandyari[3,7], Guelce Percin[8], Sandra Martin Salamanca[9], Andres Hidalgo[9,10], Claudia Waskow[8,11], Stefan Engelhardt[3,7], Andrei Todica[12], Ralf Zimmer[5], Clare Pridans[13,14], Elisa Gomez-Perdiguero[4], Christian Schulz[1,2,3]

[1]Medical Clinic I., Department of Cardiology, University Hospital, Ludwig Maximilian University, 81377 Munich, Germany

[2]Institute of Surgical Research at the Walter-Brendel-Centre of Experimental Medicine, University Hospital, Ludwig Maximilian University, 81377 Munich, Germany

[3]DZHK (German Centre for Cardiovascular Research), partner site Munich Heart Alliance, 80336 Munich, Germany

[4]Institut Pasteur, Unité Macrophages et Développement de l'Immunité, Département de Biologie du Développement et Cellules Souches, Paris, France

[5]LFE Bioinformatik, Department of Informatics, Ludwig Maximilian University, 80333 Munich, Germany

[6]Department of Neurology, Medical Faculty, Heinrich Heine University of Düsseldorf, 40225 Düsseldorf, Germany

[7]Institute of Pharmacology and Toxicology, Technical University Munich, 80802 Munich, Germany

24 [8]Immunology of Aging, Leibniz-Institute on Aging - Fritz-Lipmann-Institute (FLI), 07745 Jena,
25 Germany
26 [9]Area of Cell & Developmental Biology, Centro Nacional de Investigaciones Cardiovasculares
27 Carlos III, Madrid, Spain
28 [10]Vascular Biology and Therapeutics Program and Department of Immunobiology, Yale
29 University School of Medicine, New Haven, CT, USA
30 [11]Faculty of Biological Sciences, Friedrich-Schiller-University, 07737 Jena, Germany
31 [12]Department of Nuclear Medicine, Ludwig Maximilian University, 81377 Munich, Germany
32 [13]University of Edinburgh Centre for Inflammation Research, The Queen's Medical Research
33 Institute, Edinburgh EH16 4TJ, United Kingdom.
34 [14]Simons Initiative for the Developing Brain, Centre for Discovery Brain Sciences, University of
35 Edinburgh, Edinburgh EH8 9XD, United Kingdom
36
37 Corresponding author: Dr. Christian Schulz, MD
38 Address: Medical Clinic I., Department of Cardiology, University Hospital, Ludwig Maximilian
39 University, Marchioninistrasse 15, 81377 Munich, Germany
40 Phone: +49 89 440073092
41 Email: Christian.schulz@med.un-muenchen.de
42
43 ***Conflict-of-interest statement:*** The authors have declared that no conflict of interest exists.

ABSTRACT

Cardiac macrophages are heterogenous in phenotype and functions, which has been associated with differences in their ontogeny. Despite extensive research, our understanding of the precise role of different subsets of macrophages in ischemia/reperfusion injury remains incomplete. We here investigated macrophage lineages and ablated tissue macrophages in homeostasis and after I/R injury in a CSF1R-dependent manner. Genomic deletion of a fms-intronic regulatory element (FIRE) in the Csf1r locus resulted in specific absence of resident homeostatic and antigen-presenting macrophages, without affecting the recruitment of monocyte-derived macrophages to the infarcted heart. Specific absence of homeostatic, monocyte-independent macrophages altered the immune cell crosstalk in response to injury and induced proinflammatory neutrophil polarization, resulting in impaired cardiac remodelling without influencing infarct size. In contrast, continuous CSF1R inhibition led to depletion of both resident and recruited macrophage populations. This augmented adverse remodelling after I/R and led to an increased infarct size and deterioration of cardiac function. In summary, resident macrophages orchestrate inflammatory responses improving cardiac remodelling, while recruited macrophages determine infarct size after I/R injury. These findings attribute distinct beneficial effects to different macrophage populations in the context of myocardial infarction.

61 **GRAPHICAL ABSTRACT**

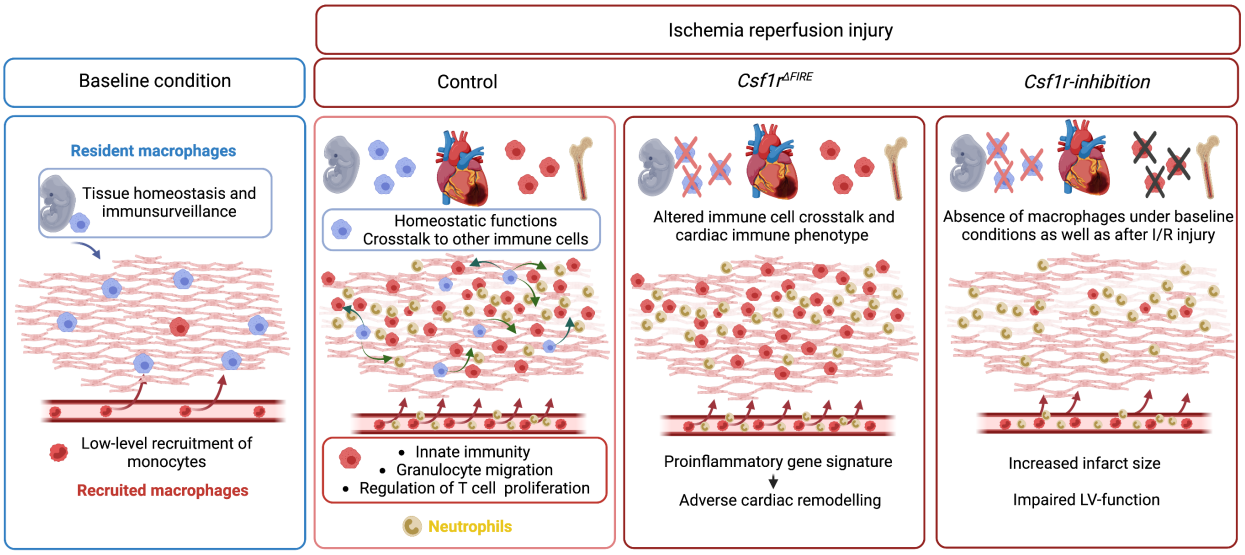

62

63

64 **INTRODUCTION**

65 Macrophages are important effectors of innate immunity. They are essential for host
66 defense against infections but are also involved in different cardiovascular diseases. They represent
67 the most abundant immune cell population in healthy cardiovascular tissues (Heidt *et al*, 2014;
68 Weinberger *et al*, 2020), where they contribute to organ functions (Hulsmans *et al*, 2017) and
69 maintenance of tissue homeostasis (Nicolas-Avila *et al*, 2020). In cardiovascular diseases such as
70 atherosclerosis and its main sequelae, ischemic stroke and acute myocardial infarction (AMI),
71 macrophage functions are central to both disease development and healing. AMI has remained a
72 leading cause of mortality and morbidity worldwide (Ahmad & Anderson, 2021; Lozano *et al*,
73 2012). Although acute survival in this condition has improved through the broad availability of
74 percutaneous coronary intervention, adverse myocardial remodeling and fibrosis frequently result
75 in heart failure (Gerber *et al*, 2016). Pathophysiologically, the diminished blood supply to
76 myocardial tissue during AMI leads to acute tissue necrosis, which induces a profound sterile
77 inflammation and triggers complex cascade of immune processes and tissue remodeling
78 (Hilgendorf *et al*, 2014; Honold & Nahrendorf, 2018; Nahrendorf *et al*, 2007). Consequently,
79 uncontrolled immune reactions in the course of AMI are associated with impaired wound healing
80 and adverse remodeling and can result in worsened cardiac outcome (Panizzi *et al*, 2010).

81 Macrophages play an essential role in cardiac injury, and thus represent a potential
82 therapeutic target (Hilgendorf *et al.*, 2014; Nahrendorf *et al.*, 2007). However, they are an
83 heterogeneous population (Kubota *et al*, 2019; Weinberger & Schulz, 2015; Zaman & Epelman,
84 2022), and a large body of work has shown that they can have both pro- and anti-inflammatory
85 functions. The differential roles of macrophage populations in AMI have remained incompletely
86 understood. Cardiac macrophages can derive from embryonic and adult hematopoietic progenitors

87 (Epelman *et al*, 2014). Fate mapping analyses have identified yolk sac (YS) erythro-myeloid
88 progenitors (EMPs) as a principal source of cardiac macrophages in adult life (Ginhoux *et al*,
89 2010). However, limited labeling in inducible cre reporter systems have not allowed for precisely
90 differentiating and quantifying developmental origins of cardiac macrophages. Further, targeting
91 of these macrophages has been challenging (Frieler *et al*, 2015; Ruedl & Jung, 2018).

92 In this study, we investigated the cellular identity of cardiac macrophages in association
93 with their developmental paths and their immune responses to ischemia/reperfusion (I/R) injury.
94 By combining lineage tracing with single cell RNA sequencing, we provide an in-depth analysis
95 of the differential functions of resident and recruited cardiac macrophages. We then harnessed
96 mice with genomic deletion of the fms-intronic regulatory element (FIRE) (Rojo *et al*, 2019), that
97 allowed us to specifically address populations of resident macrophages in the infarcted heart and
98 compared them to mice, in which both recruited as well as resident macrophages are depleted by
99 pharmacological inhibtion of the CSF1R-signalling pathway. Using these approaches of selective
100 macrophage depletion, we could attribute different beneficial functions to resident and also to
101 recruited macrophages which impact differently on cardiac remodeling, infarct size and cardiac
102 outcome.
103

104 **RESULTS**

105 *Absence of resident cardiac macrophages in Csf1r$^{\Delta FIRE}$ mice*

106 To quantify the contribution of YS EMPs to cardiac resident macrophages, we harnessed
107 constitutive labeling in *Rank*^{Cre};*Rosa26*^{eYFP} mice (Jacome-Galarza *et al*, 2019; Mass *et al*, 2016;
108 Percin *et al*, 2018). ~80% of cardiac macrophages expressed YFP in hearts of 12 week-old animals,
109 whereas blood monocytes were not labeled (**Fig 1A; Fig S1)**. EMP-derived microglia served as
110 control confirming high efficiency of Cre-mediated recombination. In a comparative analysis, we
111 traced fetal and adult definitive hematopoiesis in *Flt3*^{Cre}*Rosa26*^{eYFP} mice (Gomez Perdiguero *et al*,
112 2015; Schulz *et al*, 2012), indicating that ~20% of cardiac macrophages derived from definitive
113 HSC **(Fig 1B)**. Thus, the majority of resident macrophages in the healthy heart is of early
114 embryonic origin.

115 To determine the role of resident macrophages in the mouse heart, we generated *Rank*^{Cre}*Rosa26*^{DTR}
116 mice that express the avian diphtheria toxin (DT) receptor in the EMP lineage, rendering them
117 susceptible to DT-mediated ablation. Administration of a single DT dose, however, resulted in
118 premature death of all mice (n=6) within 24 hours (**Fig S2**). The injected mice presented with a
119 systemic inflammatory response syndrome (SIRS)-like phenotype, indicating that acute depletion
120 of EMP-derived macrophages is not viable.

121 In *Csf1r*$^{\Delta FIRE}$ mice, genetic deletion of the fms-intronic regulatory element (FIRE) in the first intron
122 of the *Csf1r* gene leads to a selective absence of tissue macrophages without the developmental
123 defects observed in *Csf1r*$^{-/-}$ mice (Munro *et al*, 2020; Rojo *et al.*, 2019). We first confirmed that
124 cardiac macrophages in *Csf1r*$^{\Delta FIRE/\Delta FIRE}$ *mice* (further termed ΔFIRE) mice were reduced by ~90%
125 and the number of monocytes and neutrophils was not altered **(Fig 1C-G)**. We thus crossed the
126 ΔFIRE animals with the YS EMP fate mapping line (*Rank*^{Cre}*Rosa26*^{eYFP} mice) and showed that

127 the macrophages absent in ΔFIRE animals were EMP-derived macrophages **(Fig 1E)**, thus offering
128 a new model to investigate the role of resident macrophages in cardiac injury.

129 *Changes in the cardiac immune phenotype in Csf1r$^{\Delta FIRE}$ mice in baseline conditions*

130 To further characterize the macrophage populations absent in healthy hearts of adult ΔFIRE mice,
131 we carried out single cell RNA-sequencing (scRNA-seq) of CD45^{+} immune cells in wildtype,
132 ΔFIRE and *Rank^{Cre}Rosa26^{eYFP}* mice **(Fig 2A, Fig S3)**. We identified the presence of six
133 macrophage clusters in control mice **(Fig 2B, Fig S3)**. Two clusters of macrophages expressing
134 homeostatic (*e.g. Lyve-1, Gas6, Stab1*) and antigen presentation-related genes (*e.g. CD74, H2-*
135 *Ab1*) were specifically ablated in ΔFIRE mice **(Fig 2C)**, which largely represent YFP-expressing
136 macrophages in *Rank^{Cre}Rosa26^{eYFP}* mice **(Fig 2D).** Specifically, we mapped ~90% of *yfp*
137 transcripts to the two clusters of homeostatic and antigen presenting macrophages that were ablated
138 in ΔFIRE. Other clusters were not reduced in ΔFIRE, and also were not quantitatively represented
139 in the YS macrophage lineage tracing model, i.e. *Cx3cr1^{hi}* (2% *yfp*), *Ccr2^{low}Ly6c^{lo}* (5% *yfp*) and
140 *Ccr2^{hi}Ly6c^{hi}* (1% *yfp*) macrophages within respective clusters (**Fig 2D**). The specific impact of
141 ΔFIRE on resident macrophages is further supported by the observation, that no changes in gene
142 expression nor cell numbers were observed in *Ly6c^{hi}* monocytes and inflammatory *Ccr2^{hi}Ly6c^{hi}*
143 macrophages **(Fig 2C Fig S4)**. Together, ΔFIRE allows for investigating the role of resident
144 cardiac macrophages that are largely of YS origin.

145 Absence of resident macrophages in ΔFIRE was associated with changes in gene expression in
146 non-macrophage clusters such as *T- and B-cells* and *natural killer (NK)* cells (**Fig S5**). Further,
147 overall phagocytic capacity, as inferred by expression of phagocytosis related genes (Amorim *et*
148 *al*, 2022), was reduced (**Fig 2E**). This suggests that absence of resident macrophages is
149 accompanied by distinct changes in immune functions in the homeostatic heart.

150 *Adverse cardiac remodeling in Csf1r$^{\Delta FIRE}$ mice after I/R injury*

151 To assess the impact of the absence of resident macrophages in cardiac injury, we subjected
152 ΔFIRE mice to I/R injury and investigated remodeling and functional outcome by sequential
153 positron emission tomography (PET) imaging after 6 and 30 days **(Fig 3A)**. Function of the cardiac
154 left ventricle (LV), as determined by ejection fraction (LVEF) and stroke volume (SV), improved
155 in controls in the course of post-I/R remodeling **(Fig 3B-C)**. In contrast, LVEF and SV remained
156 unchanged or worsened in ΔFIRE mice, and longitudinal observations of mice indicated a negative
157 net effect on ejection fraction from day 6 to day 30 post I/R. Thus, absence of resident macrophages
158 negatively influenced cardiac remodeling in the course of infarct healing **(Fig 3D-G)**. Infarct size
159 as determined by viability defect (PET) and fibrotic area (histology) was not different after 30 days
160 **(Fig 3E-H)**.

161 *Recruitment of BM-derived macrophages into infarct zone of Csf1r$^{\Delta FIRE}$ mice*

162 To gain a deeper understanding of the inflammatory processes taking place in the infarcted
163 heart, we quantified macrophage distribution by immunofluorescence and flow cytometry analysis
164 of ischemic and remote areas after I/R. In ΔFIRE mice, macrophages were largely absent in the
165 remote zone of infarcted hearts **(Fig 4A)**, indicating sustained depletion of resident macrophages.
166 However, macrophages strongly increased in the infarct area and their numbers were not different
167 in both infarct and border zones between ΔFIRE and control mice **(Fig 4A)**. This indicated
168 recruitment and differentiation of ΔFIRE-independent macrophages from the circulation into these
169 regions. Indeed, complementing lineage tracing of BM HSC in *Flt3^{Cre}* mice (**Fig 4B**) and YS EMP
170 in *Rank^{Cre}* mice (**Fig 4C**) proved the recruitment of macrophages from BM HSC (Flt3 GFP+ and
171 Rank RFP-, respectively) in the early phase of I/R injury. 30 days after I/R, BM-derived
172 macrophages remained overrepresented in the infarct zone (~75% HSC contribution), and

173 differential contribution of BM HSC declined from the border zone (~50%) to the remote zone
174 (~35%) **(Fig 4D)**. Taken together, recruited BM-derived macrophages represent the main
175 population in the infarct area and their recruitment was unaltered in ΔFIRE mice. This supports
176 the notion that resident macrophages influence cardiac remodeling but recruited macrophages
177 drive infarct size after I/R.

178 *Transcriptional landscape of resident versus recruited macrophages in I/R injury*

179 To address the differential responses of resident and recruited macrophages to I/R injury, we
180 generated BM chimeric mice. We applied an irradiation-independent model using conditional
181 deletion of c-myb to deplete BM hematopoietic cells in CD45.2 mice and replace them with
182 CD45.1 donor HSC. 2 days after I/R injury, we FACS-sorted recruited ($CD45.1^+$) and resident
183 ($CD45.2^+$) macrophages and carried out bulk RNA sequencing **(Fig 5A)**. The two macrophage
184 populations exhibited profound transcriptional differences after I/R injury. Expression of
185 homeostasis-related genes like *Timd4, Lyve-1, CD163* and *Retnla* was increased in resident
186 $CD45.2^+$ macrophages **(Fig 5B, C).** Substantiating the differential regulation of macrophage
187 programs, $CD45.1^+$ macrophages increased inflammatory- and host defense-related gene ontology
188 (GO) terms (e.g. myeloid leukocyte related immunity, killing of cells), whereas $CD45.2^+$
189 macrophages upregulated development- and homeostasis-related GO terms (e.g. extracellular
190 matrix organization, vasculature development, heart muscle development) **(Fig 5D)**. GO
191 enrichment analysis further predicted that processes involved in innate (e.g. leukocyte migration,
192 regulation of defense response, response to bacterium) as well as the adaptive immunity (e.g. T
193 cell selection, T cell activation, B cell proliferation) were increased in $CD45.1^+$ macrophages after
194 infarction **(Fig 5D)**. Thus, resident and recruited macrophages provide distinct transcriptional
195 changes and inferred functions in response to I/R.

196 *Altered inflammatory patterns and immune cell communication in Csf1r$^{\Delta FIRE}$ mice*

197 To evaluate the immune response of resident and recruited macrophages to I/R injury in ΔFIRE
198 mice, we interrogated the transcription profile of CD45^{+} cells from the infarct area **(Fig 6A)**. In
199 contrast to the absence of homeostatic and antigen-presenting macrophage clusters in healthy
200 hearts of ΔFIRE mice **(Fig 2B-C)**, there were less differences in immune cell clusters between
201 ΔFIRE and control mice 2 days after I/R **(Fig 6B, C)**. Abundance of homeostatic macrophages
202 was also reduced at this time point, however, other clusters including *Ccr2^{hi}Ly6c^{hi}* inflammatory
203 macrophages were not altered, which is in line with our histological findings.

204 ΔFIRE was associated with some changes in gene expression in cardiac non-macrophage immune
205 cells. Across different clusters, including lymphocyte and neutrophil clusters, expression of anti-
206 inflammatory genes like *Chil3 (Ym1)* and *Lcn2* was reduced**.** Vice versa, expression of Bcl-family
207 genes like *Blc2a1a* and *Bcl2a1d*, which are associated with apoptosis and inflammatory pathways,
208 was higher in ΔFIRE mice **(Fig S6-8)**. Other upregulated genes were related to antigen presentation
209 (e.g.*CD74, H2-Ab1*), as identified in the *Ccr2^{lo}Ly6c^{lo},* homeostatic and *Ccr2^{hi}Ly6c^{hi}* macrophage
210 clusters **(Fig S6 and 7)**. Further, we interrogated inflammatory gene expression in neutrophils,
211 which are abundant first responders to myocardial infarction. We found that a computed score
212 summing up inflammasome activation (Amorim *et al.*, 2022) was increased in all neutrophil
213 clusters in ΔFIRE mice (**Fig 6D**). Thus, the absence of cardiac macrophages was associated with
214 altered inflammatory properties of non-macrophage immune cells in the infarcted heart.

215 Altered intercellular crosstalk of macrophages is a hallmark of cardiac inflammation. We therefore
216 assessed ligand-receptor (LR) interactions between immune cell populations after I/R injury.
217 Indeed, the number of LR interactions with neutrophils and lymphocytes, as well as the strength
218 of the macrophage-emitted communication signals was markedly reduced in homeostatic, antigen-

219 presenting and *Ccr2^{lo}Ly6c^{lo} Mø* macrophage clusters (**Fig 6E, F, Fig. S9)**. In contrast, immune
220 cell communication in BM-derived macrophage clusters (e.g. *Ccr2^{hi}Ly6c^{hi} Mø cluster,* **Fig S10***)*
221 was not different to control mice. Taken together, deficiency in resident macrophages in I/R injury
222 altered the intercellular immune crosstalk and induced a pro-inflammatory signature in e.g. cardiac
223 neutrophils. However, transcriptional profiles of BM-derived inflammatory macrophages were
224 largely unaltered. Together with our histological analysis showing the dominance of recruited BM-
225 derived macrophages in the early phase of I/R, this potentially explained the limited impact of
226 ΔFIRE on functional outcome after I/R injury.

227 *Ablation of resident and recruited macrophages severely impacts on cardiac healing after I/R*
228 *injury*

229 To test this hypothesis, we determined the effect of combined ablation of resident and recruited
230 macrophages. We therefore exposed mice to continuous treatment with the CSF1R-inhibitor
231 PLX5622 (**Fig 7A**). In healthy hearts, inhibitor treatment resulted in the absence of cardiac
232 macrophages within 3 days (**Fig S11**). We then subjected mice to I/R injury and investigated
233 outcome by sequential PET imaging and histology **(Fig 7A)**. Treatment with PLX5622 diminished
234 macrophage numbers in both remote and infarct areas in the early phase (day 2) after injury.
235 Recruitment of other myeloid cells e.g. neutrophils was not altered in this context (**Fig 7B**). This
236 effect was pronounced in the chronic phase (day 30) after I/R injury, in which macrophages were
237 largely absent in remote, border and infarct zones (**Fig 7C,D**). Absence of resident and recruited
238 macrophages was associated increased infarct size, as determined by fibrosis area (WGA
239 histology) as well as viability defect (PET), and resulted in deterioration of cardiac function **(Fig**
240 **7E-I).** Specifically, LVEF was reduced 6 days after I/R, and remained strongly impaired at 30 days
241 **(Fig 7E).**

242 Taken together, sole absence of resident macrophages had limited negative impact on cardiac
243 remodeling. Absence of both resident and recruited macrophages resulted in a significant increase
244 in infarct size and deterioration of left ventricular function after I/R injury, highlighting a beneficial
245 effect of recruited macrophages in cardiac healing.
246

247 **DISCUSSION**

248 Macrophages are key players in cardiac homeostasis and disease (Bajpai *et al*, 2019; Bajpai
249 *et al*, 2018; Dick *et al*, 2019; Epelman *et al.*, 2014; Hulsmans *et al.*, 2017; Nahrendorf *et al.*, 2007;
250 Nicolas-Avila *et al.*, 2020; Panizzi *et al.*, 2010; Sager *et al*, 2016). The precise understanding of
251 their developmental origin, their functions and their regulation could enable the identification of
252 macrophage-targeted strategies to modify inflammation in the heart. In cardiac repair after
253 myocardial infarction, macrophages have both positive and negative effects. They are critical for
254 tissue repair, angiogenesis, and inflammation regulation, but their actions need to be carefully
255 balanced to prevent excessive inflammation, scar tissue formation, and adverse remodeling. This
256 study sheds light on the differential role of resident and recruited macrophages in cardiac
257 remodeling and outcome after AMI.

258 BM-derived recruited macrophages represents a small population in the healthy heart but
259 are recruited in vast numbers to the injured myocardium after I/R injury. These recruited cells
260 exhibit substantially different transcriptional profiles in comparison to their resident counterpart,
261 and show pro-inflammatory properties. Resident macrophages remain present in the remote and
262 border zone and display a reparative gene expression profile after I/R injury. In comparison to
263 recruited macrophages, resident macrophages expressed higher levels of genes related to
264 homeostatic functions (e.g. *Lyve-1, Timd4, CD163, Stab1*). These markers have recently been
265 associated with self-renewing tissue macrophages that are maintained independently of BM
266 contribution (Dick *et al*, 2022). Biological processes associated with cardiac healing are
267 upregulated in resident macrophages (e.g. regulation of vascular development, regulation of
268 cardiomyocyte development, extracellular matrix organization). Transcriptional profiles of
269 recruited macrophages show enhanced inflammatory biological processes also in macrophages

270 harvested from the remote area, underlining their potentially detrimental influence on remote
271 cardiac injury.

272 Two recent studies addressed the role of resident macrophages using DT-mediated
273 macrophage depletion and reported impaired cardiac remodeling in chronic myocardial infarction
274 (Dick *et al.*, 2019) and after I/R injury (Bajpai *et al.*, 2019). However, DT-mediated cell ablation
275 is known to induce neutrophil recruitment and tissue inflammation (Frieler *et al.*, 2015; Oh *et al*,
276 2017; Ruedl & Jung, 2018; Sivakumaran *et al*, 2016). This inflammatory preconditioning of
277 cardiac tissue after DT-depletion is likely to impact on cardiac remodeling and influence
278 assessment of tissue macrophage functions. Genomic deletion of FIRE in the *Csf1r* gene results in
279 the near-absence of resident cardiac macrophages but circumvents the inflammatory stimulus of
280 DT-induced depletion. ΔFIRE specifically diminished homeostatic and antigen-presenting
281 macrophages. Substantiating the specificity to resident cardiac macrophages in this genetic model,
282 the amount of macrophages recruited to the infarct area after I/R injury was not affected in ΔFIRE
283 mice. Further, scRNAseq analysis revealed that gene expression of monocytes as well as
284 *Ccr2^{hi}Ly6c^{hi} and Cx3cr1^{hi}* Mϕ, representing mainly recruited immune cells, was mostly
285 unchanged in ΔFIRE compared to control mice. The specific targeting of the resident macrophage
286 population introduces an interesting in vivo model for studying their role in MI without the need
287 for inflammation-prone conditional deletion of macrophages (Frieler *et al.*, 2015).

288 Ablation of resident macrophages altered macrophage crosstalk to non-macrophage
289 immune cells, especially lymphocytes and neutrophils. This was characterized by a
290 proinflammatory gene signature, such as neutrophil expression of inflammasome-related genes
291 and a reduction in anti-inflammatory genes like *Chil3* and *Lcn2* (Gordon & Martinez, 2010; Guo
292 *et al*, 2014; Parmar *et al*, 2018). Interestingly, inflammatory polarization of neutrophils have also

293 been associated with poor outcome after ischemic brain injury (Cuartero *et al*, 2013). Clinical trials
294 in myocardial infarction patients show a correlation of inflammatory markers with extent of the
295 myocardial damage(Sanchez *et al*, 2006) and with short- and long-term mortality (Mueller *et al*,
296 2002).

297 Our study provides evidence that the absence of resident macrophages negatively
298 influences cardiac remodeling in the late postinfarction phase in ΔFIRE mice indicating their
299 biological role in myocardial healing. In the early phase after I/R injury, absence of resident
300 macrophages had no significant effect on infarct size or LV function. These observations
301 potentially indicate a protective role in the chronic phase after myocardial infarction by modulating
302 the inflammatory response, including adjacent immune cells like neutrophils or lymphocytes.

303 Deciphering in detail the specific functions of resident macrophages is of considerable
304 interest but requires both cell-specific and temporally-controlled depletion of respective immune
305 cells in injury, which to our knowledge is not available at present. These experiments could be
306 important to tailor immune-targeted treatments of myocardial inflammation and postinfarct
307 remodelling.

308 Depletion of macrophages by pharmacological inhibition of CSF1R induced the absence
309 of both resident and recruited macrophages, allowing us to determine cardiac outcome in
310 juxtaposition to the ΔFIRE mice. Continuous CSF1R inhibition induced the absence of
311 macrophages also in the infarcted area and had deleterious effect on infarct size and LV function.
312 In line with our findings, depletion of macrophages by anti-CSF1R treatment was associated with
313 worsened cardiac function in a model of pressure overload induced heart failure (Revelo *et al*,
314 2021). Controversially, a recent study in which monocytes were depleted using DT-injections in
315 *Ccr2*^{DTR} mice reported beneficial effects on cardiac outcome after MI in mice (Bajpai *et al.*, 2019).

316 An explanation of this controversy might be the timing and duration of macrophage depletion.
317 Bajpai et al. depleted recruited macrophages only in the initial phase of myocardial infarction
318 which improved cardiac healing (Bajpai *et al.*, 2019), while depletion of macrophages over a
319 longer period of time, as shown in our study, is detrimental for cardiac repair. Furhter, other
320 immune cells including neutrophils express CCR2 and may therefore be affected directly (Talbot
321 *et al*, 2015; Xu *et al*, 2017). In line with this, Ccr2-deficient mice exhibit reduced acute recruitment
322 of neutrophils to the brain after I/R injury, which was associated with reduced infarct size and
323 brain edema (Dimitrijevic *et al*, 2007).

324 Taken together our study underlines the heterogeneity of cardiac macrophages and the
325 importance of ontogeny therein. Resident macrophages, which mainly derive from YS EMPs,
326 govern cardiac homeostasis in the healthy heart, and contribute positively to cardiac healing after
327 I/R injury by orchestrating anti-inflammatory programming of other cardiac immune cells.
328 However, recruited macrophages contribute to the healing phase after AMI and their absence
329 defines infarct size and cardiac outcome.

330

331

332 **MATERIALS AND METHODS**

333 *Mice*

334 *Rank*^{Cre} (Jacome-Galarza *et al.*, 2019; Percin *et al.*, 2018), *Flt3*^{Cre} (Benz *et al*, 2008), *Myb*$^{fl/fl}$
335 (Emambokus *et al*, 2003), *Mx1*^{Cre} (Kuhn *et al*, 1995) (from The Jackson Laboratory (JAX), Stock
336 No: 003556), *Csf1r*$^{\Delta FIRE}$ (Rojo *et al.*, 2019), *Rosa26*^{DTR} (Buch *et al*, 2005) (JAX Stock No:
337 007900), *Rosa26*$^{mT/mG}$ (Muzumdar *et al*, 2007) (JAX Stock No: 007676), *Rosa26*^{eYFP} (Srinivas *et al*,
338 2001) (JAX Stock No: 006148), and *Rosa26*^{RFP} (JAX Stock No: 034720) mice have been previously
339 described. PCR genotyping was performed according to protocols described previously. Animals
340 were aged between 10-16 weeks. We have complied with all relevant ethical regulations. Animal
341 studies were approved by the local regulatory agency (Regierung von Oberbayern, Munich,
342 Germany, record numbers ROB-55.2-2532.Vet_02-19-17 and ROB-55.2-2532.Vet_02-19-1; Care
343 and Use Committee of the Institut Pasteur (CETEA), dap190119).

344 FIRE mice were kept on a CBA/Ca background. Experiments in which reporter mice were
345 necessary (*Csf1r*$^{\Delta FIRE}$*Rank*^{Cre}*Rosa26*^{eYFP}) the background was mixed with a C57Bl6 background.
346 All experiments evaluating cardiac function and outcome after infarction in FIRE mice were
347 performed on mice kept with a CBA/Ca background.

348 For fate-mapping analysis of Flt3^{+} precursors, *Flt3*^{Cre} males (the transgene is located on
349 the Y chromosome) were crossed to *Rosa26*^{eYFP} or *Rosa26*$^{mT/mG}$ female reporter mice and only the
350 male progeny was used. For all other experiments, the offspring of both sexes was used for
351 experiments.

352 BM transplantation was enabled by conditional deletion of the transcription factor *myb* as
353 previously described (Stremmel *et al*, 2018). In brief, we induced BM ablation by 4 injections of

354 polyI:C into *CD45.2; Mx1*^{Cre}*Myb*$^{flox/flox}$ every other day, and then transplanted BM from congenic
355 *C57BL/6 CD45.1* (*Ly5.1*; JAX Stock No: 006584). We confirmed the success (chimerism of above
356 90%) of the BM-transplantation after 4 weeks**.**

357 To deplete macrophages, we used the selective CSF1R-inhibitor PLX5622. Control and
358 PLX5622 (300 ppm formulated in AIN-76A standard chow, Research Diets, Inc.) chows were
359 kindly provided by Plexxikon Inc (Berkeley, CA). For depletion of RANK-lineage macrophages,
360 *Rank*^{Cre}*Rosa26*^{DTR} mice were injected intraperitoneally with 0.02 mg/kg body weight diphtheria
361 toxin (DT; Sigma-Aldrich) at the timepoints mentioned in Fig ure and corresponding legend. Mice
362 were closely monitored by veterinarians and according to score sheets that were approved by the
363 regulatory agency. Single DT application in *Rank*^{Cre}*Rosa26*^{DTR} mice let to rapid deterioration of
364 their health (without infarction or other interventions), and consequently experiments needed to be
365 aborted according to regulations; experimental outcomes were then documented as premature
366 death as indicated.

367 *Ischemia-reperfusion (I/R) injury*

368 I/R injury was carried out as previously described (Novotny *et al*, 2018). In brief, mice
369 were anesthetized using 2% isoflurane and intraperitoneal injection of fentanyl (0.05 mg/kg),
370 midazolam (5.0 mg/kg) and medetomidine (0.5 mg/kg), and then intubated orally (MiniVent
371 Ventilator model nr. 845, Harvard Apparatus®) and ventilated (volume of 150 µL at 200/min).
372 After lateral thoracotomy, the left anterior descending artery (LAD) was ligated with an 8-0
373 prolene suture producing an ischemic area in the apical left ventricle (LV). To induce the
374 reperfusion injury, the suture was removed after 60 min and reperfusion was confirmed by
375 observing the recoloring of the LV. Postoperative analgesia was performed by injection of

376 Buprenorphin (0.1 mg/kg) twice per day for 3 days. After 2, 6 or 30 days after I/R injury organs
377 were harvested after cervical dislocation.

378 *Organ harvest*

379 Mice were anaesthetized using 2% isoflurane and organ harvest was performed after
380 cervical dislocation. Blood was harvested with a heparinized syringe (2mL) by cardiac puncture.
381 After perfusion with 20 mL of ice-cold PBS hearts were excised and kept in PBS on ice until
382 further tissue processing. For flow cytometry, hearts were divided into the ischemia (tissue distal
383 of the LAD ligation) and remote area (tissue proximal of the LAD ligation). For histological
384 examinations of tissues, hearts were incubated in 4% PFA for 30 min followed by an incubation
385 in 30% sucrose-solution (Sigma Aldrich®) for 24 h. Afterwards, hearts were mounted onto a heart
386 slicing device and cut transversally into 3 equal parts (termed level 1, 2 and 3) and stored in Tissue-
387 Tek® (Sakura Finetek Germany GmbH) at -80°C.

388 *Immunohistology*

389 Cryosections (10-12 µm) of heart tissue were fixed with 4% paraformaldehyde for 10 min.
390 Blocking and permeabilization were performed with 0.5% Saponin and 10% goat serum for 1h.
391 Primary antibodies were added and incubated for 2-18 h (see Supplemental Table 1). Slides were
392 washed with PBS and secondary antibodies were added and incubated for 1h (see Supplemental
393 Table 1). WGA-staining (Wheat Germ Agglutinin Alexa Fluor™ 647 conjugated antibody,
394 ThermoFisher Scientific®) was used to locate and measure the infarct area and nuclei were stained
395 with DAPI. Finally, slides were washed one more time and Fluorescence Mounting Medium was
396 used to cover the stained sample.

397 Heart samples were evaluated using an Axio Imager M2 (Carl Zeiss®) and blinded picture
398 analysis was performed using ZEN Imaging and Axiovision SE64 Rel. 4.9.1 (Carl Zeiss®). For
399 the evaluation of cell numbers, 6 individual high-resolution images from each respective
400 anatomical region (infarct area, border zone and remote zone) were analysed for each animal. To
401 measure infarct size the heart was cut into 3 parts and the infarcted area was measured as WGA^+
402 area in sections from each part.

403 *Flow cytometry*

404 100 µL of heparinized blood was used for FACS analysis. Erythrocytes were lysed with
405 1% ammonium chloride. After washing with PBS, the cell suspension was resuspended in purified
406 rat anti-mouse CD16/CD32 (BD Pharmingen®) and incubated for 15 min at 4°C. Following this,
407 cells were incubated with FACS-antibodies for 15 min at 4°C **(table S1)**.

408 Heart tissue was dissected into remote and ischemic tissue as described above and minced
409 into small pieces using forceps and a scalpel. When comparing baseline and I/R injury in FACS
410 analysis, basal heart tissue was used for comparison with remote tissue and apical heart tissue for
411 comparison with ischemia tissue. After enzymatic digestion (Collagenase XI 1200 U/mg,
412 Collagenase I 125 U/mg, Hyaluronidase 500 U/mg, DNase I 1836 U/mg; Sigma Aldrich®) for 30
413 min at 37°C cells were washed and incubated with purified anti-CD16/32 (FcγRIII/II; dilution
414 1/50) for 10 min. Thereafter, cells were incubated wit FACS-antibodies (**table S1**) for 30 min at
415 4°C. FACS-analysis was performed on a BD Fortessa® or a BeckmanCoulter Cytoflex® flow
416 cytometer and gating strategies are shown in Supplemental Fig ures 1 and 3. Data were analysed
417 using FlowJo® (version 10.0.8r1).

418 *Cell Sorting*

419 Cell sorting was performed on a MoFlo Astrios (Beckman Coulter) to obtain cardiac
420 macrophages from *CD45.2; Mx1*^{Cre}*Myb*$^{flox/flox}$ after BM-transplantation of CD45.1 BM (n=3 for 2
421 days after I/R injury) for bulk sequencing, or all cardiac immune cells (CD45^{+} cells) of *Csf1r*$^{\Delta FIRE}$
422 and *Rank*^{Cre}*Rosa26*^{eYFP} mice (n=3 for *Csf1r*$^{\Delta FIRE/+}$ and *Csf1r*$^{\Delta FIRE/\Delta FIRE}$ in baseline conditions, n=1
423 for *Rank*^{Cre}*Rosa26*^{eYFP} in baseline conditions; n=2 for *Csf1r*$^{\Delta FIRE/+}$ and *Csf1r*$^{\Delta FIRE/\Delta FIRE}$ 2 days after
424 I/R injury) for single cell analysis. CD45^{+} cells were enriched by using magnetic beads and MS
425 columns (CD45 MicroBeads; Miltenyi Biotec). Cells were then sorted as single/live/CD45^{+} cells
426 for single cell sequencing from baseline hearts and from the ischemic myocardium 2 days after I/R
427 injury. Bulk sequencing was performed on single/live/CD45^{+}/lin^{-}
428 /CD11b^{+}/F4/80^{+}/CD64^{+}/CD45.1^{+} or CD45.2^{+} cells from the remote and the ischemic myocardium
429 2 days after I/R injury. Dead cells were identified with SYTOX Orange Dead Cell Stain.

430 *Bulk sequencing and analysis*

431 For each sample, ~1000 macrophages were sorted into 75µL of RLT buffer (Qiagen,
432 containing 1% beta-mercaptoethanol), vortexed for 1 min and immediately frozen (-80°C). RNA
433 extraction (RNeasy® Plus Micro Kit, Qiagen), cDNA generation (SMART®-Seq v4 Ultra Low
434 Input RNA Kit, Takara Bio) and library preparation (Nextera® XT DNA Library Prep Kit,
435 Illumina) were performed according to the manufacturer's specifications. Sequencing was
436 performed on a HiSeq4000 system (Ilumina).

437 The obtained reads were trimmed using bbduk from the BBMap
438 (https://sourceforge.net/projects/bbmap/) v38.87 collection using parameters "ktrim=r k=23
439 mink=11 hdist=1 tpe tbo". The trimmed reads were aligned with Hisat2 2.2.1 against the Ensembl
440 release 102 reference mouse genome (Yates *et al*, 2020).

441 Gene expression was quantified using the featureCounts (Liao *et al*, 2014) application from
442 the subread package (v2.0.1) and with parameters "--primary -O -C -B -p -T 8 --minOverlap 5".
443 Differential expression analysis was performed using DESeq2 (v1.30.0) (Love *et al*, 2014). A
444 Gene Ontology Set Enrichment analysis was performed using the ClusterProfiler R package
445 (v3.18.1). The visualization of the respective clustermaps was layouted using the ForceAtlas2
446 implementation of the python fa2 (https://pypi.org/project/fa2/) package for networkx (v2.5)
447 (https://networkx.org/).

448 On the library-size normalized count data, the pymRMR ((Peng *et al*, 2005),
449 https://pypi.org/project/pymrmr/) package was used to derive the top 100 discriminatory genes
450 (Mutual Information Quotient method) for subsequently calculating the UMAP 2D-embedding (
451 (McInnes *et al*, 2020), (https://pypi.org/project/umap-learn/)) for all samples (umap-learn package
452 v0.5.0rc1, 3 neighbors) ((McInnes *et al*, 2018), https://pypi.org/project/pymrmr/).

453 *Single cell RNA sequencing and analysis*

454 After sorting, cells were proceeded for single cell capture, barcoding and library
455 preparation using Chromium Next GEM single cell 3' (v3.1, 10x Genomics) according to
456 manufacturer's specifications. Pooled libraries were sequenced on an Illumina HiSeq1500
457 sequencer (Illumina, San Diego, USA) in paired-end mode with asymmetric read length of 28+91
458 bp and a single indexing read of 8bp.

459 The reads of heart1 sample ($Rank^{Cre}Rosa26^{eYFP}$) were demultiplexed using Je-
460 demultiplex-illu (Girardot *et al*, 2016) and mapped against a customized mouse reference genome
461 (GRCm38.p6, Gencode annotation M24) including eYfp sequence using CellRanger (v3.1.0, 10x
462 Genomics).

463 The six mouse samples 20133-0001 to 20133-0006 (baseline condition of *Csf1r*$^{\Delta FIRE/+}$ and
464 *Csf1r*$^{\Delta FIRE/\Delta FIRE}$), were processed using Cellranger 4.0.0 using the 2020A mm10 reference.

465 The 4 mouse samples (MUC13956-13959, infarct condition of *Csf1r*$^{\Delta FIRE/+}$ and
466 *Csf1r*$^{\Delta FIRE/\Delta FIRE}$), were sequenced with 4 technical sequencing replicates and pooled using the
467 cellranger (v4.0.0, 10x Genomics) pipeline. Cellranger 4.0.0 was called with default parameters
468 and the 2020A mm10 reference for gene expression.

469 Finally, all 11 samples were integrated using Seurat 4.0.0 (on R 4.0.1) (Stuart & Satija,
470 2019). The samples were processed, and cells were filtered to contain between 200 and 6000
471 features, have at least 1000 molecules detected (nCount_RNA > 1000), have below 15% mtRNA
472 content (^MT) and below 40% ribosomal RNA content (^Rps|^Rpl). After this filtering a total of
473 35759 cells remained.

474 After performing SCTransform (Hafemeister & Satija, 2019) on the samples, the SCTransform
475 vignette for integrating the datasets was followed (with 2000 integration features). For
476 dimensionality reduction, PCA was performed using default parameters, and UMAP and
477 Neighbour-Finding was run on 50 PCs. Clustering was performed at a resolution of 0.8. A total of
478 18 clusters was identified using this approach. Cluster markers were calculated using the t-test in
479 the FindMarkers function. Subsequently cell types were initially predicted using the cPred cell
480 type prediction (https://github.com/mjoppich/scrnaseq_celltype_prediction). Upon manual
481 curation, further fine-grained cell type annotations were made. Differential comparisons were
482 performed against several subgroups of the data set. These comparisons were performed using the
483 t-test in the FindMarkers function of Seurat. Differential results are visualized using the
484 EnhancedVolcano library (Blighe K, 2021).

485 For the analysis of cell-cell interactions we downloaded the ligand-receptor pairs from Jin
486 et al. (Jin *et al*, 2021) from the Lewis Lab GitHub repository
487 (https://github.com/LewisLabUCSD/Ligand-Receptor-Pairs). For each interaction (ligand-
488 receptor pair for a cluster-pair) the communication score is calculated as the expression product
489 (Armingol *et al*, 2021) of the mean normalized expressions exported from the Seurat object. This
490 ensures that little expression of either ligand or receptor in only one cluster results in a relatively
491 low communication score, and only good expression of ligand and receptor will result in a high
492 communication score. The direction of an interaction is fixed from ligand to receptor. The single
493 ligand-receptor-communication-scores were then aggregated (sum) such that only interactions
494 with a score greater six were taken into account.

495 Gene module scores for inflammasome, ROS and phagocytosis gene sets were calculated
496 using Seurat's AddModuleScore function. All scripts, including the ones for creating the
497 visualizations of bulk and scRNA-seq data, are available online through
498 https://github.com/mjoppich/myocardial_infarction .

499 *In Vivo PET Imaging*

500 ECG-gated positron emission tomography (PET) images were performed on day 6 and 30
501 after I/R injury of the LAD using a dedicated small-animal PET scanner (Inveon Dedicated PET,
502 Preclinical Solutions, Siemens Healthcare Molecular Imaging, Knoxville, TN, USA), as
503 previously described (Brunner *et al*, 2012). Anaesthesia was induced with isoflurane (2.5%),
504 delivered via a face mask in pure oxygen at a rate of 1.2 L/min and maintained with isoflurane
505 (1.5%). Approximately 15 MBq 2-deoxy-2-[18F]fluoro-D-glucose ([18F]-FDG) (~100 µL) were
506 administered through a teil vein catheter and slowly flushed immediately afterwards with 50 µL
507 saline solution. Body temperature was monitored using a rectal thermometer and maintained

508 within the normal range using a heating pad. After placing animals within the aperture of the PET
509 scanner ECG electrodes (3M, St. Paul, MN, USA) were placed on both forepaws and the left hind
510 paw and ECG was recorded using a dedicated physiological monitoring system (BioVet; Spin
511 Systems Pty Ltd., Brisbane, Australia) (Todica *et al*, 2018). The PET emission acquisition (list-
512 mode) was initiated 30 min after [18F]-FDG injection and lasted 15 min (Brunner *et al.*, 2012;
513 Gross *et al*, 2016). For scatter and attenuation correction and additional 7-min long transmission
514 scan was performed using a Co-57 source.

515 The accuracy of the ECG trigger signal was verified retrospectively using in-house
516 software programmed in MATLAB (The Mathworks, Natick, USA) and in C programming
517 language and erroneous trigger events were removed when needed, as previously described
518 (Boning *et al*, 2013). Further processing of the data was performed using the Inveon Acquisition
519 Workplace (Siemens Medical Solutions, Knoxville, TN). As previously described, data was
520 reconstructed as a static image or as a cardiac gated image with 16 bins in a 128 × 128 matrix with
521 a zoom of 211% using an OSEM 3D algorithm with 4 and a MAP 3D algorithm with 32 iterations
522 (Brunner *et al.*, 2012). The reconstructed data was normalized, corrected for randoms, dead time
523 and decay as well as attenuation and scatter.

524 PET images were analysed using the Inveon Research Workplace in a blinded manner (Siemens
525 Medical Solutions, Knoxville, TN). Infarct sizes were determined from static reconstructed images
526 using QPS® (Cedars-Sinai, Los Angeles, CA, USA). Hereby, datasets were compared to a
527 normative database and the viability defect was calculated as percentage of the left ventricular
528 volume, as described previously (Lehner *et al*, 2014; Todica *et al*, 2014). Left ventricular function
529 volumes (EDV, ESV, SV), as well as the LVEF, were determined from ECG-gated images using

530 QGS® (Cedars-Sinai, Los Angeles, CA, USA), as described previously (Brunner *et al.*, 2012;
531 Croteau *et al*, 2003).

532 *Statistical analysis*

533 Student's t-test or Fisher's LSD test was used (Prism GraphPad®). Welch's correction for
534 unequal variances was used when applicable. A p-value of $p < 0.05$ was considered significant.
535 The Shapiro-Wilk test was used to test normality. Data are presented as mean +/- standard
536 deviation (SD).

537

ACKNOLEDGEMENTS

We thank Nicole Blount, Beate Jantz, Michael Lorenz, Sebastian Helmer for excellent technical assistance.

FUNDING:

DZHK (German Centre for Cardiovascular Research) and the BMBF (German Ministry of Education and Research) (grants 81Z0600204 to CS, 81X2600252 to TW and 81X2600256 to MF). The Deutsche Forschungsgemeinschaft (SCHU 2297/1-1 and collaborative research centers 1123 project Z02 (MJ, RZ) and A07 (CS), and CRC TRR332 project A6 (CS). LMUexcellent (TW). ESC Research Grant 2021 (TW). Friedrich-Baur Stiftung (TW). Deutsche Stiftung für Herzforschung (M.F.). Chinese Scholarship Council (CSC) to JF and LL.

AUTHOR CONTRIBUTIONS:

Conceptualization: TW, CSchu

Methodology: TW, MJ, MF, JL, GP, AT, DE, CSchu

Investigation: TW, DM, MJ, MF, CG, KK, VW, SR, SA, JF, LL, WHL, JW, LT, DE, GP, SMS

Funding acquisition: TW, MF, RZ, EGP, CSchu

Supervision: AH, CW, SE, AT, RZ, CP, EGP, CSchu

Writing – original draft: TW, MJ

Writing – review & editing: all authors

Conflict of interest:

The authors declare no conflict of interest.

559 **References**

560 Ahmad FB, Anderson RN (2021) The Leading Causes of Death in the US for 2020. *JAMA*
561 Amorim A, De Feo D, Friebel E, Ingelfinger F, Anderfuhren CD, Krishnarajah S, Andreadou M, Welsh CA, Liu Z,
562 Ginhoux F *et al* (2022) IFNgamma and GM-CSF control complementary differentiation programs in the monocyte-
563 to-phagocyte transition during neuroinflammation. *Nat Immunol* 23: 217-228
564 Armingol E, Officer A, Harismendy O, Lewis NE (2021) Deciphering cell-cell interactions and communication
565 from gene expression. *Nat Rev Genet* 22: 71-88
566 Bajpai G, Bredemeyer A, Li W, Zaitsev K, Koenig AL, Lokshina I, Mohan J, Ivey B, Hsiao HM, Weinheimer C *et*
567 *al* (2019) Tissue Resident CCR2- and CCR2+ Cardiac Macrophages Differentially Orchestrate Monocyte
568 Recruitment and Fate Specification Following Myocardial Injury. *Circ Res* 124: 263-278
569 Bajpai G, Schneider C, Wong N, Bredemeyer A, Hulsmans M, Nahrendorf M, Epelman S, Kreisel D, Liu Y, Itoh A
570 *et al* (2018) The human heart contains distinct macrophage subsets with divergent origins and functions. *Nat Med*
571 24: 1234-1245
572 Benz C, Martins VC, Radtke F, Bleul CC (2008) The stream of precursors that colonizes the thymus proceeds
573 selectively through the early T lineage precursor stage of T cell development. *J Exp Med* 205: 1187-1199
574 Blighe K RS, Lewis M, 2021. EnhancedVolcano: Publication-ready volcano plots with enhanced colouring and
575 labeling. R package version 1.10.0, https://githubcom/kevinblighe/EnhancedVolcano
576 Boning G, Todica A, Vai A, Lehner S, Xiong G, Mille E, Ilhan H, la Fougere C, Bartenstein P, Hacker M (2013)
577 Erroneous cardiac ECG-gated PET list-mode trigger events can be retrospectively identified and replaced by an
578 offline reprocessing approach: first results in rodents. *Phys Med Biol* 58: 7937-7959
579 Brunner S, Todica A, Boning G, Nekolla SG, Wildgruber M, Lehner S, Sauter M, Ubleis C, Klingel K, Cumming P
580 *et al* (2012) Left ventricular functional assessment in murine models of ischemic and dilated cardiomyopathy using
581 [18 F]FDG-PET: comparison with cardiac MRI and monitoring erythropoietin therapy. *EJNMMI Res* 2: 43
582 Buch T, Heppner FL, Tertilt C, Heinen TJ, Kremer M, Wunderlich FT, Jung S, Waisman A (2005) A Cre-inducible
583 diphtheria toxin receptor mediates cell lineage ablation after toxin administration. *Nat Methods* 2: 419-426
584 Croteau E, Benard F, Cadorette J, Gauthier ME, Aliaga A, Bentourkia M, Lecomte R (2003) Quantitative gated PET
585 for the assessment of left ventricular function in small animals. *J Nucl Med* 44: 1655-1661
586 Cuartero MI, Ballesteros I, Moraga A, Nombela F, Vivancos J, Hamilton JA, Corbi AL, Lizasoain I, Moro MA
587 (2013) N2 neutrophils, novel players in brain inflammation after stroke: modulation by the PPARgamma agonist
588 rosiglitazone. *Stroke* 44: 3498-3508
589 Dick SA, Macklin JA, Nejat S, Momen A, Clemente-Casares X, Althagafi MG, Chen J, Kantores C, Hosseinzadeh
590 S, Aronoff L *et al* (2019) Self-renewing resident cardiac macrophages limit adverse remodeling following
591 myocardial infarction. *Nat Immunol* 20: 29-39
592 Dick SA, Wong A, Hamidzada H, Nejat S, Nechanitzky R, Vohra S, Mueller B, Zaman R, Kantores C, Aronoff L *et*
593 *al* (2022) Three tissue resident macrophage subsets coexist across organs with conserved origins and life cycles. *Sci*
594 *Immunol* 7: eabf7777
595 Dimitrijevic OB, Stamatovic SM, Keep RF, Andjelkovic AV (2007) Absence of the chemokine receptor CCR2
596 protects against cerebral ischemia/reperfusion injury in mice. *Stroke* 38: 1345-1353
597 Emambokus N, Vegiopoulos A, Harman B, Jenkinson E, Anderson G, Frampton J (2003) Progression through key
598 stages of haemopoiesis is dependent on distinct threshold levels of c-Myb. *EMBO J* 22: 4478-4488
599 Epelman S, Lavine KJ, Beaudin AE, Sojka DK, Carrero JA, Calderon B, Brija T, Gautier EL, Ivanov S, Satpathy
600 AT *et al* (2014) Embryonic and adult-derived resident cardiac macrophages are maintained through distinct
601 mechanisms at steady state and during inflammation. *Immunity* 40: 91-104
602 Frieler RA, Nadimpalli S, Boland LK, Xie A, Kooistra LJ, Song J, Chung Y, Cho KW, Lumeng CN, Wang MM *et*
603 *al* (2015) Depletion of macrophages in CD11b diphtheria toxin receptor mice induces brain inflammation and
604 enhances inflammatory signaling during traumatic brain injury. *Brain Res* 1624: 103-112
605 Gerber Y, Weston SA, Enriquez-Sarano M, Berardi C, Chamberlain AM, Manemann SM, Jiang R, Dunlay SM,
606 Roger VL (2016) Mortality Associated With Heart Failure After Myocardial Infarction: A Contemporary
607 Community Perspective. *Circ Heart Fail* 9: e002460
608 Ginhoux F, Greter M, Leboeuf M, Nandi S, See P, Gokhan S, Mehler MF, Conway SJ, Ng LG, Stanley ER *et al*
609 (2010) Fate mapping analysis reveals that adult microglia derive from primitive macrophages. *Science* 330: 841-845
610 Girardot C, Scholtalbers J, Sauer S, Su SY, Furlong EE (2016) Je, a versatile suite to handle multiplexed NGS
611 libraries with unique molecular identifiers. *BMC Bioinformatics* 17: 419

612 Gomez Perdiguero E, Klapproth K, Schulz C, Busch K, Azzoni E, Crozet L, Garner H, Trouillet C, de Bruijn MF,
613 Geissmann F *et al* (2015) Tissue-resident macrophages originate from yolk-sac-derived erythro-myeloid
614 progenitors. *Nature* 518: 547-551
615 Gordon S, Martinez FO (2010) Alternative activation of macrophages: mechanism and functions. *Immunity* 32: 593-
616 604
617 Gross L, Paintmayer L, Lehner S, Brandl L, Brenner C, Grabmaier U, Huber B, Bartenstein P, Theiss HD, Franz
618 WM *et al* (2016) FDG-PET reveals improved cardiac regeneration and attenuated adverse remodelling following
619 Sitagliptin + G-CSF therapy after acute myocardial infarction. *Eur Heart J Cardiovasc Imaging* 17: 136-145
620 Guo H, Jin D, Chen X (2014) Lipocalin 2 is a regulator of macrophage polarization and NF-kappaB/STAT3
621 pathway activation. *Mol Endocrinol* 28: 1616-1628
622 Hafemeister C, Satija R (2019) Normalization and variance stabilization of single-cell RNA-seq data using
623 regularized negative binomial regression. *Genome Biol* 20: 296
624 Heidt T, Courties G, Dutta P, Sager HB, Sebas M, Iwamoto Y, Sun Y, Da Silva N, Panizzi P, van der Laan AM *et al*
625 (2014) Differential contribution of monocytes to heart macrophages in steady-state and after myocardial infarction.
626 *Circ Res* 115: 284-295
627 Hilgendorf I, Gerhardt LM, Tan TC, Winter C, Holderried TA, Chousterman BG, Iwamoto Y, Liao R, Zirlik A,
628 Scherer-Crosbie M *et al* (2014) Ly-6Chigh monocytes depend on Nr4a1 to balance both inflammatory and
629 reparative phases in the infarcted myocardium. *Circ Res* 114: 1611-1622
630 Honold L, Nahrendorf M (2018) Resident and Monocyte-Derived Macrophages in Cardiovascular Disease. *Circ Res*
631 122: 113-127
632 Hulsmans M, Clauss S, Xiao L, Aguirre AD, King KR, Hanley A, Hucker WJ, Wulfers EM, Seemann G, Courties G
633 *et al* (2017) Macrophages Facilitate Electrical Conduction in the Heart. *Cell* 169: 510-522 e520
634 Jacome-Galarza CE, Percin GI, Muller JT, Mass E, Lazarov T, Eitler J, Rauner M, Yadav VK, Crozet L, Bohm M *et*
635 *al* (2019) Developmental origin, functional maintenance and genetic rescue of osteoclasts. *Nature* 568: 541-545
636 Jin S, Guerrero-Juarez CF, Zhang L, Chang I, Ramos R, Kuan CH, Myung P, Plikus MV, Nie Q (2021) Inference
637 and analysis of cell-cell communication using CellChat. *Nat Commun* 12: 1088
638 Kubota A, Suto A, Suzuki K, Kobayashi Y, Nakajima H (2019) Matrix metalloproteinase-12 produced by
639 Ly6C(low) macrophages prolongs the survival after myocardial infarction by preventing neutrophil influx. *J Mol*
640 *Cell Cardiol* 131: 41-52
641 Kuhn R, Schwenk F, Aguet M, Rajewsky K (1995) Inducible gene targeting in mice. *Science* 269: 1427-1429
642 Lehner S, Todica A, Vanchev Y, Uebleis C, Wang H, Herrler T, Wangler C, Cumming P, Boning G, Franz WM *et*
643 *al* (2014) In vivo monitoring of parathyroid hormone treatment after myocardial infarction in mice with
644 [68Ga]annexin A5 and [18F]fluorodeoxyglucose positron emission tomography. *Mol Imaging* 13: 1-8
645 Liao Y, Smyth GK, Shi W (2014) featureCounts: an efficient general purpose program for assigning sequence reads
646 to genomic features. *Bioinformatics* 30: 923-930
647 Love MI, Huber W, Anders S (2014) Moderated estimation of fold change and dispersion for RNA-seq data with
648 DESeq2. *Genome Biol* 15: 550
649 Lozano R, Naghavi M, Foreman K, Lim S, Shibuya K, Aboyans V, Abraham J, Adair T, Aggarwal R, Ahn SY *et al*
650 (2012) Global and regional mortality from 235 causes of death for 20 age groups in 1990 and 2010: a systematic
651 analysis for the Global Burden of Disease Study 2010. *Lancet* 380: 2095-2128
652 Mass E, Ballesteros I, Farlik M, Halbritter F, Gunther P, Crozet L, Jacome-Galarza CE, Handler K, Klughammer J,
653 Kobayashi Y *et al* (2016) Specification of tissue-resident macrophages during organogenesis. *Science* 353
654 McInnes L, Healy J, Melville J (2020) UMAP: Uniform Manifold Approximation and Projection for Dimension
655 Reduction. *arXiv*
656 McInnes L, Healy J, Saul N, Großberger L (2018) UMAP: Uniform Manifold Approximation and Projection. *J*
657 *Open Source Softw* 3, (29), 861
658 Mueller C, Buettner HJ, Hodgson JM, Marsch S, Perruchoud AP, Roskamm H, Neumann FJ (2002) Inflammation
659 and long-term mortality after non-ST elevation acute coronary syndrome treated with a very early invasive strategy
660 in 1042 consecutive patients. *Circulation* 105: 1412-1415
661 Munro DAD, Bradford BM, Mariani SA, Hampton DW, Vink CS, Chandran S, Hume DA, Pridans C, Priller J
662 (2020) CNS macrophages differentially rely on an intronic Csf1r enhancer for their development. *Development* 147
663 Muzumdar MD, Tasic B, Miyamichi K, Li L, Luo L (2007) A global double-fluorescent Cre reporter mouse.
664 *Genesis* 45: 593-605
665 Nahrendorf M, Swirski FK, Aikawa E, Stangenberg L, Wurdinger T, Figueiredo JL, Libby P, Weissleder R, Pittet
666 MJ (2007) The healing myocardium sequentially mobilizes two monocyte subsets with divergent and
667 complementary functions. *J Exp Med* 204: 3037-3047

668 Nicolas-Avila JA, Lechuga-Vieco AV, Esteban-Martinez L, Sanchez-Diaz M, Diaz-Garcia E, Santiago DJ, Rubio-
669 Ponce A, Li JL, Balachander A, Quintana JA *et al* (2020) A Network of Macrophages Supports Mitochondrial
670 Homeostasis in the Heart. *Cell* 183: 94-109 e123
671 Novotny J, Chandraratne S, Weinberger T, Philippi V, Stark K, Ehrlich A, Pircher J, Konrad I, Oberdieck P, Titova
672 A *et al* (2018) Histological comparison of arterial thrombi in mice and men and the influence of Cl-amidine on
673 thrombus formation. *PloS one* 13: e0190728
674 Oh DS, Oh JE, Jung HE, Lee HK (2017) Transient Depletion of CD169(+) Cells Contributes to Impaired Early
675 Protection and Effector CD8(+) T Cell Recruitment against Mucosal Respiratory Syncytial Virus Infection. *Front*
676 *Immunol* 8: 819
677 Panizzi P, Swirski FK, Figueiredo JL, Waterman P, Sosnovik DE, Aikawa E, Libby P, Pittet M, Weissleder R,
678 Nahrendorf M (2010) Impaired infarct healing in atherosclerotic mice with Ly-6C(hi) monocytosis. *J Am Coll*
679 *Cardiol* 55: 1629-1638
680 Parmar T, Parmar VM, Perusek L, Georges A, Takahashi M, Crabb JW, Maeda A (2018) Lipocalin 2 Plays an
681 Important Role in Regulating Inflammation in Retinal Degeneration. *J Immunol* 200: 3128-3141
682 Peng H, Long F, Ding C (2005) Feature selection based on mutual information: criteria of max-dependency, max-
683 relevance, and min-redundancy. *IEEE Trans Pattern Anal Mach Intell* 27: 1226-1238
684 Percin GI, Eitler J, Kranz A, Fu J, Pollard JW, Naumann R, Waskow C (2018) CSF1R regulates the dendritic cell
685 pool size in adult mice via embryo-derived tissue-resident macrophages. *Nat Commun* 9: 5279
686 Revelo X, Parthiban P, Chen C, Barrow F, Fredrickson G, Wang H, Yucel D, Herman A, van Berlo JH (2021)
687 Cardiac Resident Macrophages Prevent Fibrosis and Stimulate Angiogenesis. *Circ Res*
688 Rojo R, Raper A, Ozdemir DD, Lefevre L, Grabert K, Wollscheid-Lengeling E, Bradford B, Caruso M, Gazova I,
689 Sanchez A *et al* (2019) Deletion of a Csf1r enhancer selectively impacts CSF1R expression and development of
690 tissue macrophage populations. *Nat Commun* 10: 3215
691 Ruedl C, Jung S (2018) DTR-mediated conditional cell ablation-Progress and challenges. *Eur J Immunol* 48: 1114-
692 1119
693 Sager HB, Hulsmans M, Lavine KJ, Moreira MB, Heidt T, Courties G, Sun Y, Iwamoto Y, Tricot B, Khan OF *et al*
694 (2016) Proliferation and Recruitment Contribute to Myocardial Macrophage Expansion in Chronic Heart Failure.
695 *Circ Res* 119: 853-864
696 Sanchez PL, Rodriguez MV, Villacorta E, Albarran C, Cruz I, Moreiras JM, Martin F, Pabon P, Fernandez-Aviles F,
697 Martin-Luengo C (2006) [Kinetics of C-reactive protein release in different forms of acute coronary syndrome]. *Rev*
698 *Esp Cardiol* 59: 441-447
699 Schulz C, Gomez Perdiguero E, Chorro L, Szabo-Rogers H, Cagnard N, Kierdorf K, Prinz M, Wu B, Jacobsen SE,
700 Pollard JW *et al* (2012) A lineage of myeloid cells independent of Myb and hematopoietic stem cells. *Science* 336:
701 86-90
702 Sivakumaran S, Henderson S, Ward S, Sousa PS, Manzo T, Zhang L, Conlan T, Means TK, D'Aveni M, Hermine O
703 *et al* (2016) Depletion of CD11c(+) cells in the CD11c.DTR model drives expansion of unique CD64(+) Ly6C(+)
704 monocytes that are poised to release TNF-alpha. *Eur J Immunol* 46: 192-203
705 Srinivas S, Watanabe T, Lin CS, William CM, Tanabe Y, Jessell TM, Costantini F (2001) Cre reporter strains
706 produced by targeted insertion of EYFP and ECFP into the ROSA26 locus. *BMC Dev Biol* 1: 4
707 Stremmel C, Schuchert R, Schneider V, Weinberger T, Thaler R, Messerer D, Helmer S, Geissmann F, Frampton J,
708 Massberg S *et al* (2018) Inducible disruption of the c-myb gene allows allogeneic bone marrow transplantation
709 without irradiation. *J Immunol Methods* 457: 66-72
710 Stuart T, Satija R (2019) Integrative single-cell analysis. *Nat Rev Genet* 20: 257-272
711 Talbot J, Bianchini FJ, Nascimento DC, Oliveira RD, Souto FO, Pinto LG, Peres RS, Silva JR, Almeida SC,
712 Louzada-Junior P *et al* (2015) CCR2 Expression in Neutrophils Plays a Critical Role in Their Migration Into the
713 Joints in Rheumatoid Arthritis. *Arthritis Rheumatol* 67: 1751-1759
714 Todica A, Beetz NL, Gunther L, Zacherl MJ, Grabmaier U, Huber B, Bartenstein P, Brunner S, Lehner S (2018)
715 Monitoring of Cardiac Remodeling in a Mouse Model of Pressure-Overload Left Ventricular Hypertrophy with
716 [(18)F]FDG MicroPET. *Mol Imaging Biol* 20: 268-274
717 Todica A, Zacherl MJ, Wang H, Boning G, Jansen NL, Wangler C, Bartenstein P, Kreissl MC, Hacker M, Brunner
718 S *et al* (2014) In-vivo monitoring of erythropoietin treatment after myocardial infarction in mice with
719 [(6)(8)Ga]Annexin A5 and [(1)(8)F]FDG PET. *J Nucl Cardiol* 21: 1191-1199
720 Weinberger T, Esfandyari D, Messerer D, Percin G, Schleifer C, Thaler R, Liu L, Stremmel C, Schneider V,
721 Vagnozzi RJ *et al* (2020) Ontogeny of arterial macrophages defines their functions in homeostasis and
722 inflammation. *Nat Commun* 11: 4549

723 Weinberger T, Schulz C (2015) Myocardial infarction: a critical role of macrophages in cardiac remodeling. *Front*
724 *Physiol* 6: 107
725 Xu P, Zhang J, Wang H, Wang G, Wang CY, Zhang J (2017) CCR2 dependent neutrophil activation and
726 mobilization rely on TLR4-p38 axis during liver ischemia-reperfusion injury. *Am J Transl Res* 9: 2878-2890
727 Yates AD, Achuthan P, Akanni W, Allen J, Allen J, Alvarez-Jarreta J, Amode MR, Armean IM, Azov AG, Bennett
728 R *et al* (2020) Ensembl 2020. *Nucleic Acids Res* 48: D682-D688
729 Zaman R, Epelman S (2022) Resident cardiac macrophages: Heterogeneity and function in health and disease.
730 *Immunity* 55: 1549-1563
731

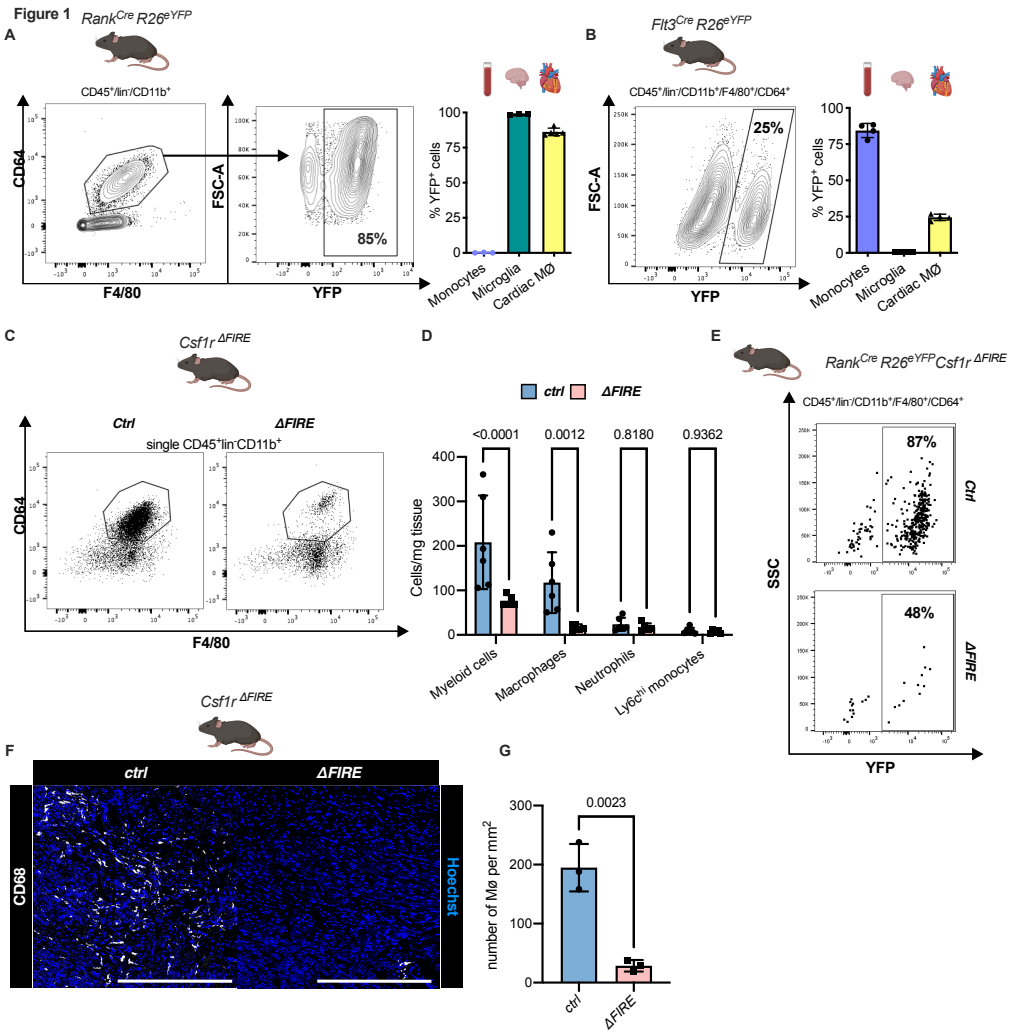

Figure 1. Absence of resident cardiac macrophages in *Csf1r*$^{\Delta FIRE}$ mice.
(A) Flow cytometry analysis of 3 month-old *Rank*^{Cre}*Rosa26*^{eYFP} mice, showing single/CD45^{+}/lin-(CD11c, Ter119, Tcrß, Nk1.1)/CD11b^{+} cardiac cells, eYFP expression in macrophages (CD64^{+}/F4/80^{+}) and percentage of eYFP^{+} blood monocytes, microglia and cardiac macrophages (n=3-5 each from an independent experiment). (B) Flow cytometry analysis of 3 month-old *Flt3*^{Cre}*Rosa26*^{eYFP} mice, showing macrophage expression of eYFP and percentage of eYFP^{+} blood monocytes, microglia and cardiac macrophages (n=4 each from an independent experiment). **(C)** Representative flow cytometry analysis of cardiac macrophages in *control* and Δ*FIRE mice* **(D)** Quantification of myeloid cells by flow cytometry (CD45^{+}/lin^{-}/CD11b^{+}), macrophages (CD45^{+}/lin^{-}/CD11b^{+}/CD64^{+}/F4/80^{+}), neutrophils (CD45^{+}/lin^{-}/CD11b^{+}/CD64^{-}/F4/80^{-}/Ly6g^{+}) and Ly6c^{hi} monocytes (CD45^{+}/lin^{-}/CD11b^{+}/CD64^{-}/F4/80^{-}/Ly6g-/Ly6c^{hi}) (*n=6 for control* and n=5 for Δ*FIRE* mice, each single experiments). **(E)** Representative flow cytometry analysis of cardiac macrophages and their expression of eYFP in *Csf1r*$^{\Delta FIRE/+}$*Rank*^{Cre}*Rosa26*^{eYFP} *and* *Csf1r*$^{\Delta FIRE/\Delta FIRE}$*Rank*^{Cre}*Rosa26*^{eYFP}. **(F)** Representative immunohistological images showing macrophages (CD68^{+} cells in white and Hoechst in blue) in *control* and Δ*FIRE* hearts in 3 month-old mice at baseline conditions (scale bars represent 500µm). **(F)** Quantification of macrophages by histology ((*n=3 for control* and Δ*FIRE* mice). Either Fisher's LSD test or unpaired t-test were performed and mean ± SD is shown.

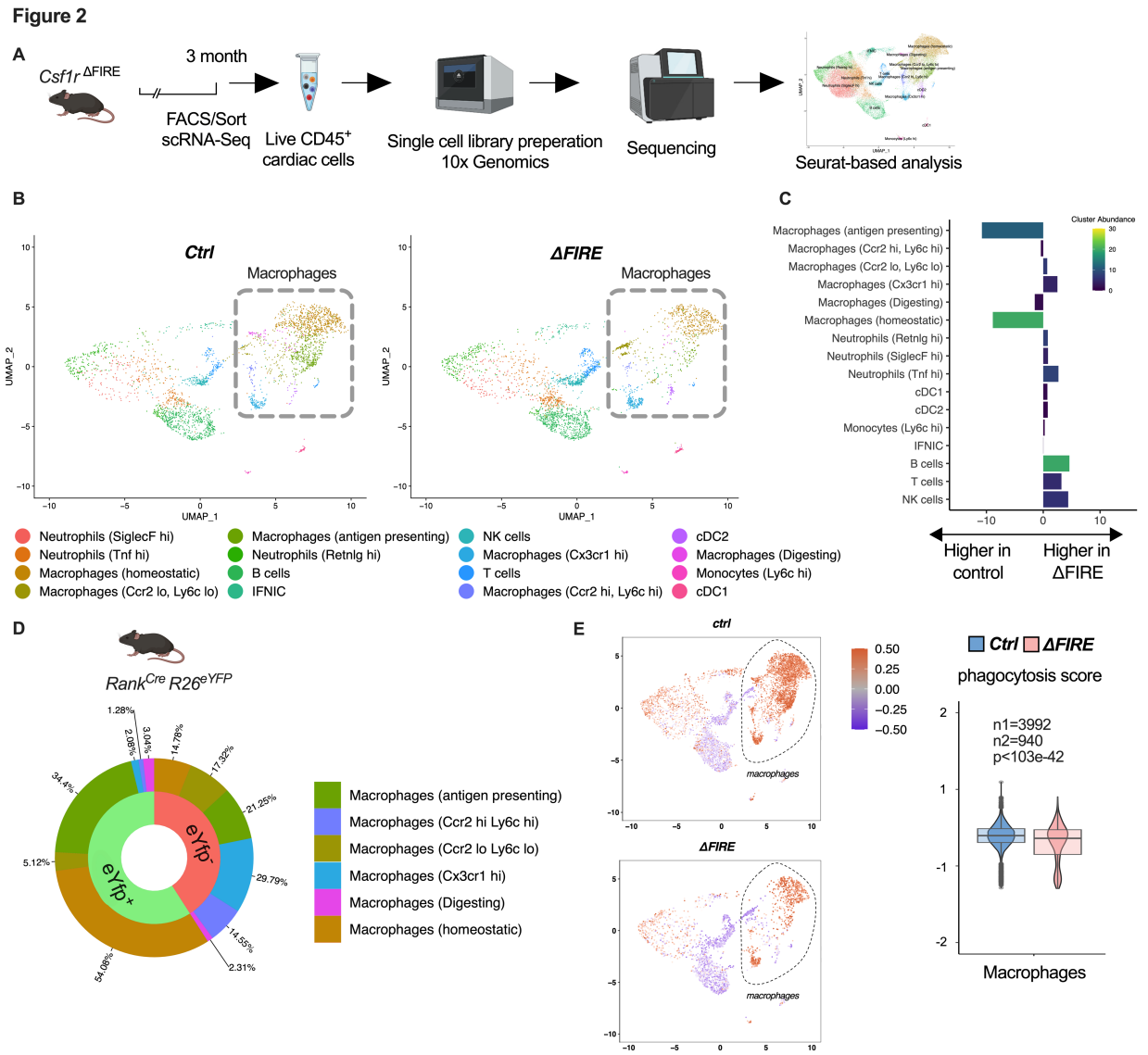

Figure 2. Changes in the cardiac immune phenotype in *Csf1r*$^{\Delta FIRE}$ mice in baseline conditions. **(A)** Experimental setup to analyze cardiac immune cells using scRNA-seq of sorted CD45^{+}/live cells. **(B)** UMAPs of control and ΔFIRE in baseline conditions (n=3 for *control* and Δ*FIRE)* **(C)** Absolute difference (percentage points) in cluster abundance between *control* and Δ*FIRE*. **(D)** Contribution of EMP-derived (*eYfp* expressing) macrophages to the different macrophage clusters analysed by scRNA-seq analysis of immune cells harvested from a *Rank*^{Cre}*Rosa26*^{eYFP} mouse. **(E)** Phagocytosis score projected on a UMAP displaying *control and* Δ*FIRE* immune cell subsets. Violin and box plots show the computed phagocytosis score combined in all macrophage clusters (n1/n2 represents number of cells from control/ Δ*FIRE* mice).

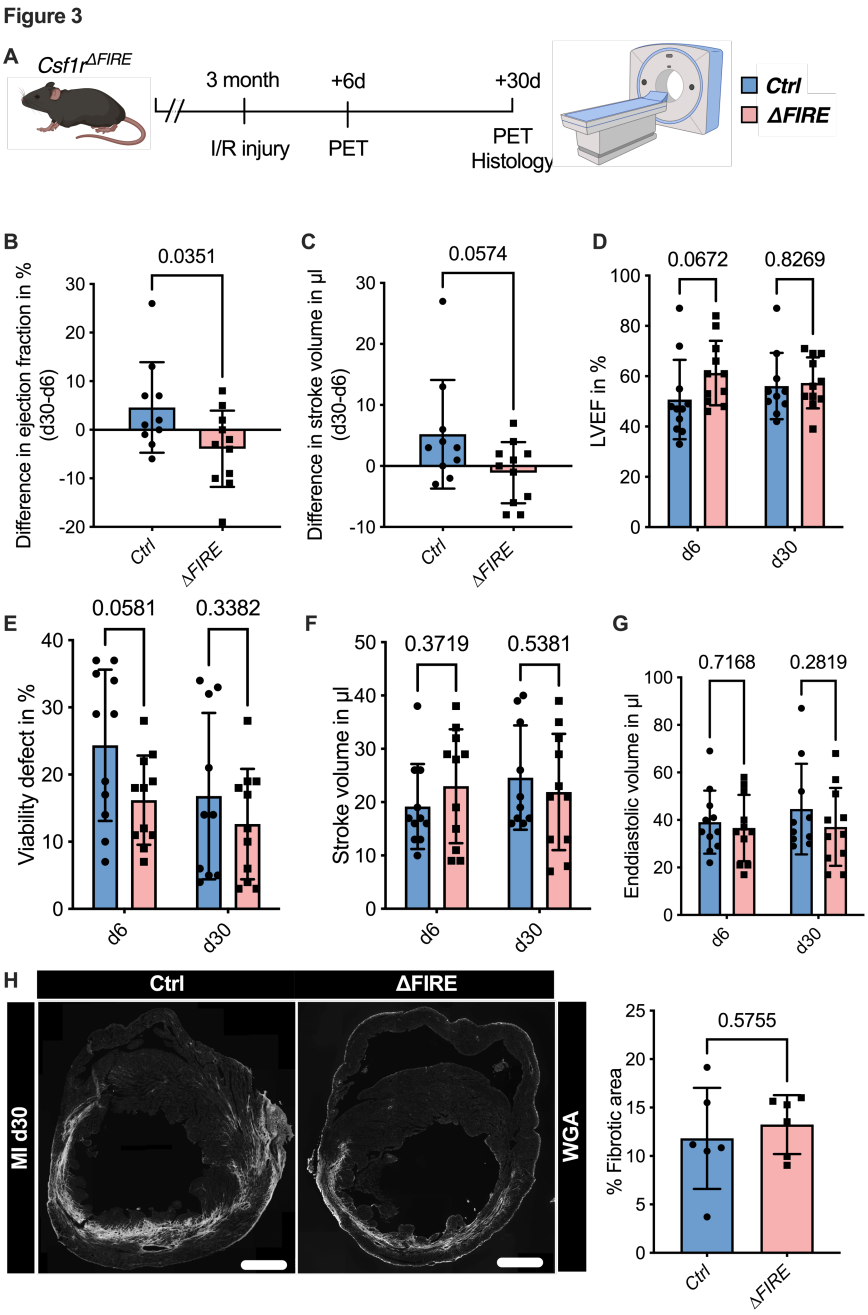

Figure 3. Adverse cardiac remodeling in *Csf1r*$^{\Delta FIRE}$ mice after I/R injury

(A) Schematic of the sequential analysis of cardiac function, dimensions and viability using positron-emission tomography 6 and 30 days after I/R injury in *control* and Δ*FIRE* with (B and C) showing the intraindividual changes in each parameter from d6 to d30 and (D-G) the individual timepoints on d6 and d30 (d6: n=11 for *control and* Δ*FIRE*, d30: n=10 for *control and n=11 for* Δ*FIRE*). **(B and D)** left ventricular ejection fraction (LVEF), **(C and E)** percentage of the viability defect, **(F)** stroke volume and **(F)** left-ventricular end-diastolic volume**. (H**) Representative immunohistological images showing the fibrotic area (WGA^{+} area) in hearts from *control and ΔFIRE* mice 30 days after I/R injury. Right panel shows the percentage of fibrotic area in the respective groups (n= 6 for each group). Student's t-test was performed and mean ± SD is shown.

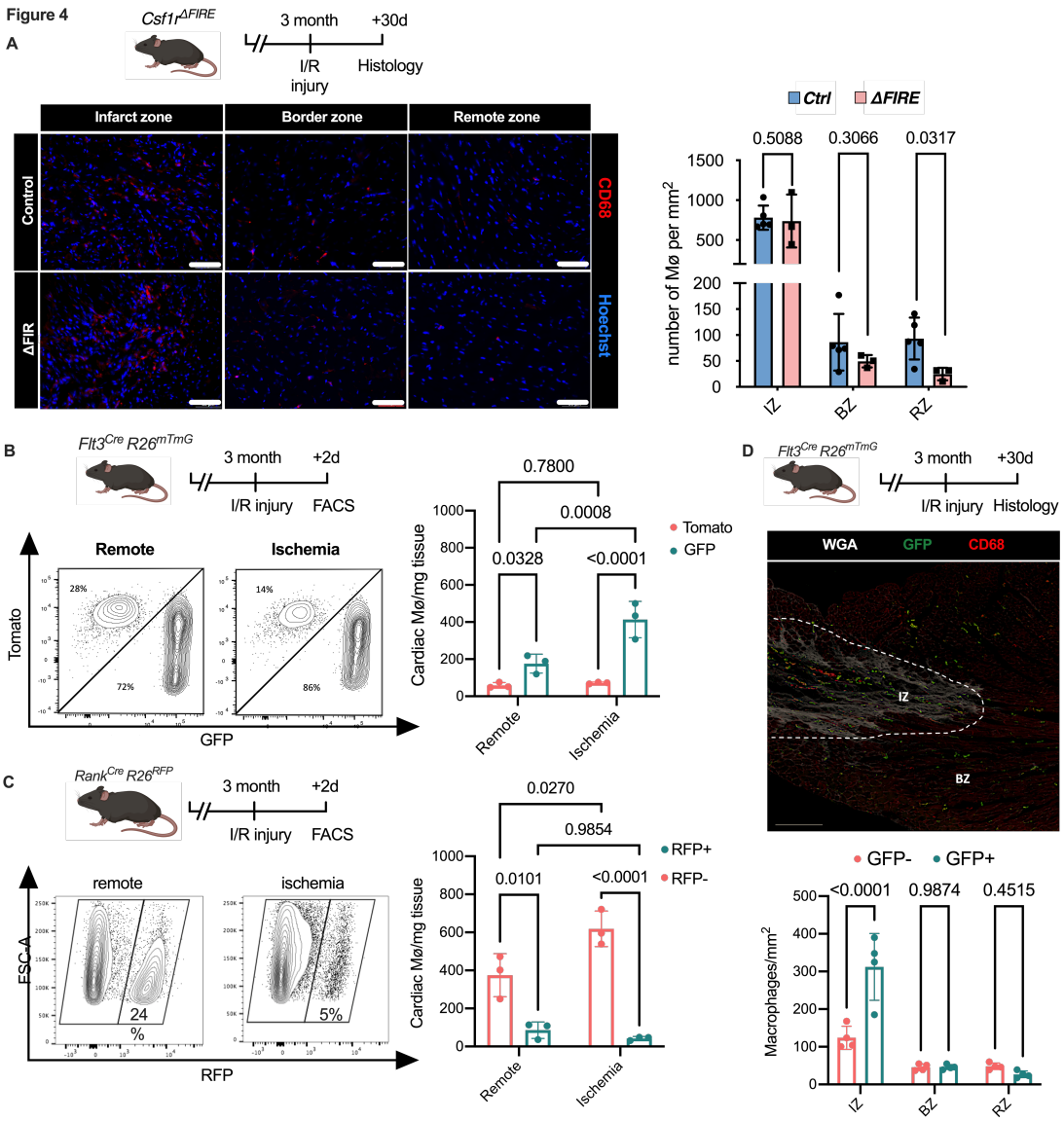

Figure 4. Recruitment of BM-derived macrophages into infarct zone of *Csf1r*$^{\Delta FIRE}$ mice. **(A)** Representative immunohistology of hearts from Δ*FIRE* mice 30 days after I/R injury showing macrophages (CD68^{+} cells in red and Hoechst in blue) in the infarct, border and remote zone. Right panel shows number of cardiac macrophages in the respective area (n=5 *control* and n=3 for Δ*FIRE*). **(B)** Flow cytometry analysis of *Flt3*^{Cre}*Rosa26*$^{mT/mG}$ mice 2 days after I/R injury, (left) representative flow cytometry showing expression of tomato and GFP in macrophages in the remote and ischemic myocardium and (right) number of tomato^{+} and GFP^{+} cardiac macrophages in the respective area (n=3, each individual experiments). **(C)** Flow cytometry analysis of *Rank*^{Cre}*Rosa26*^{RFP} mice 2 days after I/R injury, (left) representative flow cytometry showing expression of RFP in macrophages in the remote and ischemic myocardium and (right) number of RFP^{-} and RFP^{+} cardiac macrophages in the respective area (n=3, each individual experiments). **(D)** Histological analysis of *Flt3*^{Cre}*Rosa26*$^{mT/mG}$ mice 30 days after I/R injury in the infarct, border and remote zone, (left) representative immunohistology of the infarct and border zone and (right) number of GFP^{-} and GFP^{+} cardiac macrophages in the respective areas (n=4). Fishers LSD test was performed for all experiments and mean ± SD is shown.

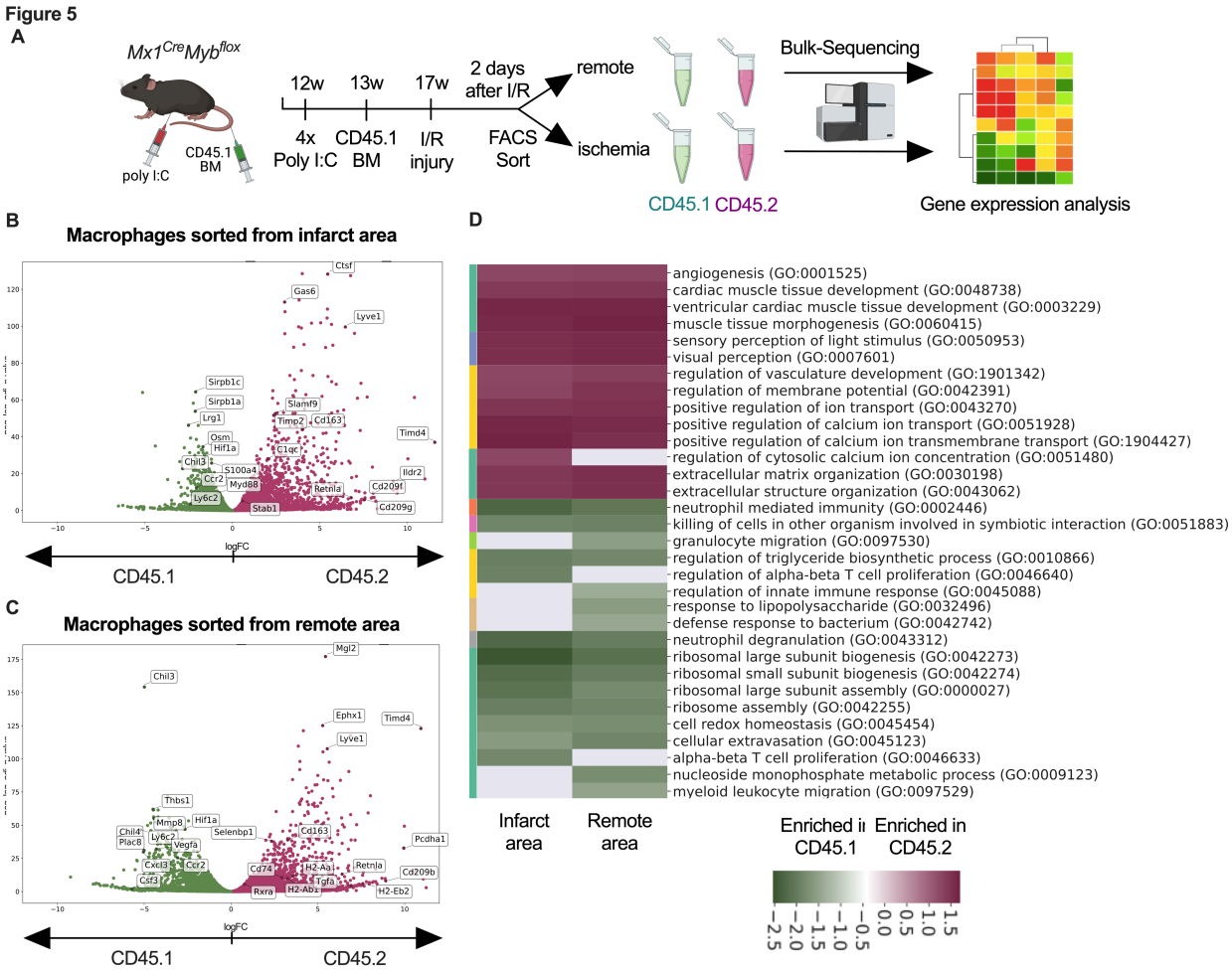

Figure 5. Transcriptional landscape of resident versus recruited macrophages in I/R injury **(A)** Experimental setup to generate non-irradiation BM chimera using *CD45.2 Mx1*^{Cre}*Myb*$^{flox/flox}$ and transplantation of CD45.1 BM. I/R injury was induced 4 weeks after BM-transplantation and CD45.1^{+} and CD45.2^{+} macrophages were sorted from the remote and ischemic myocardium 2 days after I/R injury and RNA-sequencing was performed on bulk cells (n=3)**. (B and C)** Volcano plot showing differential gene expression analysis results of recruited CD45.1 vs. resident CD45.2 macrophages in the **(B)** remote and **(C)** ischemic zone. **(D)** Gene ontology enrichment analysis showing specific biological processes enriched in CD45.1 and CD45.2 macrophages in the ischemic and remote zone.

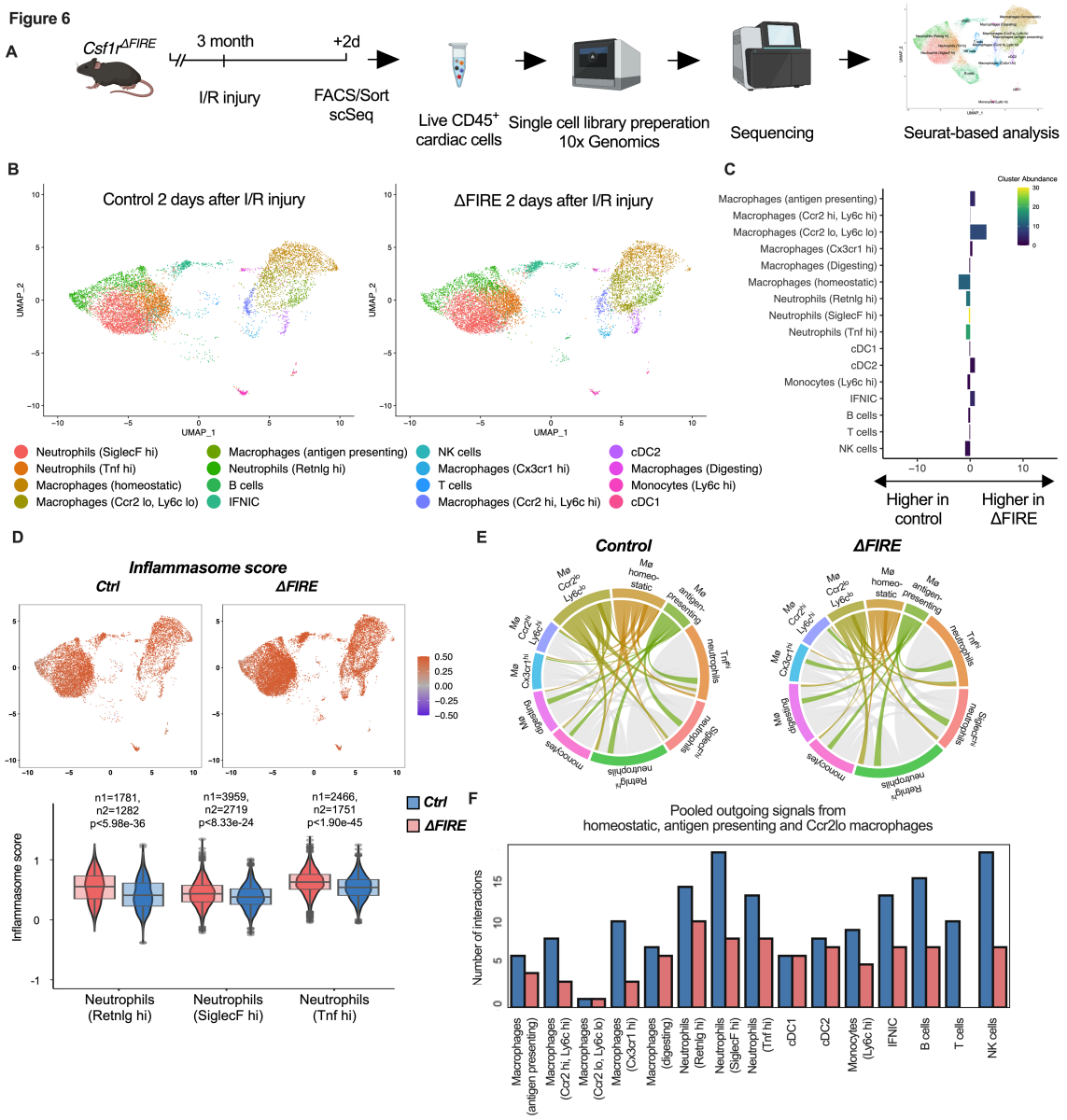

Figure 6. **Altered inflammatory patterns and immune cell communication in *Csf1r*$^{\Delta FIRE}$ mice.** **(A)** Experimental setup to analyze transcriptional changes in cardiac immune cells on a single cell level 2 days after I/R injury in *ΔFIRE* mice. **(B)** UMAPs of control and ΔFIRE 2 days after I/R injury (n=2 for *control* and Δ*FIRE)*. **(C)** Absolute difference (percentage points) in cluster abundance between *control* and Δ*FIRE*. **(D)** Inflammasome score projected on a UMAP displaying control and ΔFIRE immune cell subsets after I/R injury. Violin and box plots show the computed inflammasome score in neutrophil clusters (n1/n2 represents number of cells from control/ Δ*FIRE* mice). (**E**) Ligand–receptor interactions of *antigen-presenting, Ccr2*^{lo} *ly6c*^{lo} *and homeostatic macrophages* (highlighted) with other immune cell clusters. Shown are the aggregated communication scores (width of interactions) for all cell types. Only communication scores larger than 6 are considered. (**F**) Number of interactions (with communication score > 6) outgoing from homeostatic, antigen presenting and Ccr2^{lo} macrophages to other immune cell clusters.

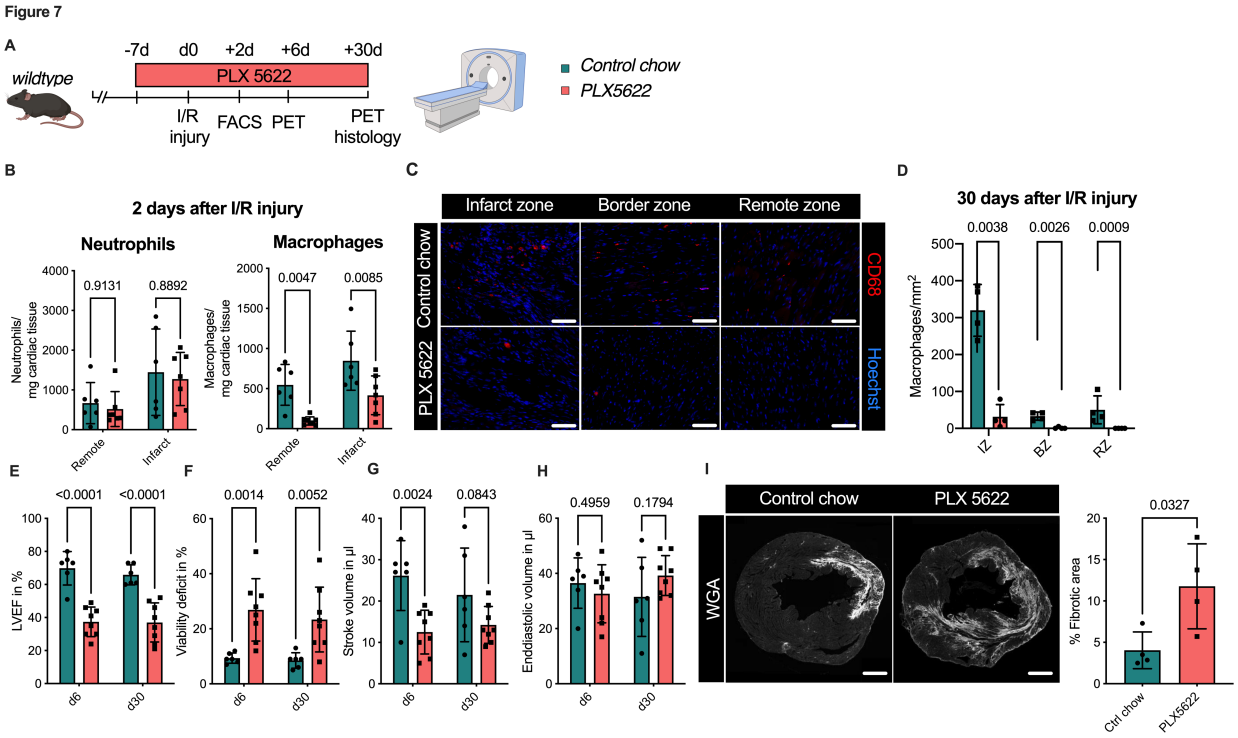

Figure 7. **Ablation of resident and recruited macrophages severely impacts on cardiac healing after I/R injury**

(A) Schematic of the analysis of cardiac function and infarct size in mice treated with PLX5622 7 days prior and 30 days after I/R injury. **(B)** Number of cardiac macrophages and neutrophils in the remote and ischemic myocardium 2 days after I/R injury in mice fed control chow (n=6) or PLX5622 (n=7). **(C)** Representative immunohistology of hearts 30 days after I/R injury showing macrophages ($CD68^+$ cells in red and Hoechst in blue) in the infarct, border and remote zone and **(D)** number of cardiac macrophages in the respective area (n=4 for control chow and n=4 for PLX5622). **(E)** Left ventricular ejection fraction (LVEF), **(F)** viability deficit, **(G)** stroke volume and **(H)** end-diastolic volume measured using positron-emission tomography 6 and 30 days after I/R injury (n=6 for control chow, n=8 for PLX5622). **(I)** Representative immunohistological images showing the fibrotic area (WGA^+ area) in hearts 30 days after I/R injury from mice fed control chow or PLX5622. Percentage of fibrotic area in the respective groups (n= 4 for each group). Student's t-test or Fishers LSD test was performed and mean ± SD is shown.